Decomposition of high-rank factorized unitary coupled-cluster operators using ancilla and multiqubit controlled low-rank counterparts

Luogen Xu,[1] Joseph T. Lee,[2] and J. K. Freericks[1]
[1]*Department of Physics, Georgetown University, 37th and O Streets NW, Washington, DC 20057, USA*
[2]*Department of Applied Physics and Mathematics, Columbia University, 500 West 120th Street, New York, New York 10027, USA*

(Received 12 November 2021; accepted 9 December 2021; published 4 January 2022)

The factorized form of the unitary coupled-cluster (UCC) approximation is one of the most promising methodologies to prepare trial states for strongly correlated systems within the variational quantum eigensolver framework. The factorized form of the UCC *Ansatz* can be systematically applied to a reference state to generate the desired entanglement. The difficulty associated with such an approach is the requirement of simultaneously entangling a growing number of qubits, which quickly exceeds the hardware limitations of today's quantum machines. In particular, while circuits for singles and double excitations can be performed on current hardware, higher-rank excitations require too many gate operations. In this work, we propose a set of schemes that trade off using extra qubits for a reduced gate depth to decompose high-rank UCC excitation operators into significantly lower depth circuits. These results will remain useful even when fault-tolerant machines are available to reduce the overall state-preparation circuit depth.

DOI: 10.1103/PhysRevA.105.012406

I. INTRODUCTION

Efficiently simulating quantum many-body systems on quantum hardware is one of the major goals of quantum computation, and many algorithms already exist [1–4] for this problem. For weakly correlated systems seen in many quantum chemistry systems, there is a hierarchy to the amplitudes of the determinants in the expansion of the ground-state wave function—low-rank excitations from the reference state typically have larger amplitudes than higher-rank excitations. But, generically, many determinants are still needed to achieve chemical accuracy even with this hierarchy. When the number of electrons and spin orbitals is small enough, the molecule can be treated by exact diagonalization, which is called the full configuration interaction [5] in the chemistry field. But very few systems can be treated this way on classical computers due to the exponential growth of the Hilbert space scaling as $O(2^N)$. Truncating the Hilbert space to include the most important many-body basis states is called the configuration-interaction (CI) method. But it suffers from not being size consistent, which affects the accuracy when molecules are stretched close to the dissociation limit. Instead, the coupled-cluster (CC) method [6] provides high precision, is size consistent, and is lean on memory usage because it does not explicitly construct the wave function. The CC method scales as $O(N^{10})$ when including singles, doubles, triples, and quadruples.

The variational quantum eigensolver (VQE) algorithm relies on the variational principle of quantum mechanics to estimate the ground-state energy of a molecule [7]. While the VQE can be used for physical systems in condensed matter and other fields of physics, the main application is in quantum chemistry. Classical quantum chemistry methods boast high accuracy but can be expensive. Thus, one active area of research is in leveraging quantum technology to calculate the ground-state energy of molecules.

Picking the proper wave-function *Ansatz* is one of the more difficult challenges not only in using VQE for quantum chemistry but also in other approaches in which a trial wave function is needed [8]. The classical coupled-cluster approximation applies an exponential operator to the reference state (typically, the Hartree-Fock wave function). In conventional CC calculations, one applies the coupled-cluster operator as a similarity transformation of the Hamiltonian. Because the Hamiltonian contains only single and two-particle interactions, the power series expansion of the similarity transformation truncates after at most fourfold nested commutator terms, which proves to be efficient when carried out on classical computers. However, most operations applicable to quantum machines must be unitary. This suggests using the unitary coupled-cluster (UCC) *Ansatz* [9,10], which includes a sum of excitations minus deexcitations, to have a unitary operator applied to the reference state. Unfortunately, the similarity transformation of the Hamiltonian under the UCC *Ansatz* does not truncate after a small number of terms. Strategies used to evaluate it on classical computers include truncating the series at a fixed order [9], expanding the exponential operator in a power series and truncating the series when higher-order terms no longer change the wave function [11], and using an exact operator identity of the factorized form of the UCC to allow the wave function to be constructed in a tree structure [12]. If $\hat{T}$ is the operator that is exponentiated in the traditional CC approach and applied to the reference state, i.e., $|\psi_{\rm CC}\rangle = \exp(\hat{T})\,|\psi_0\rangle$, the corresponding UCC *Ansatz* is the unitary variant, given by $|\psi_{\rm UCC}\rangle = \exp(\hat{T} - \hat{T}^\dagger)\,|\psi_0\rangle$. Note that the $\hat{T}$ operator

involves fermionic destruction operators for the real orbitals (present in the reference state) and an equal number of fermionic creation operators for the virtual operators (corresponding to orbitals that can be occupied in the expansion of the wave function). So the $\hat{T}$ operator excites the reference state. The operator $\hat{T}^\dagger$ annihilates against the reference state, but it can be nonzero when it acts on other determinants in the expansion for the wave function. The standard way to implement the UCC approximation is to exponentiate the sum of all the different excitation and deexcitation operators $\hat{T} - \hat{T}^\dagger$ via

$$\hat{U}_{\rm UCC} = e^{\hat{T}-\hat{T}^\dagger} = e^{\sum \theta^{abc\cdots}_{ijk\cdots}[\hat{A}^{abc\cdots}_{ijk\cdots} - (\hat{A}^{abc\cdots}_{ijk\cdots})^\dagger]}, \tag{1}$$

where we define the excitation operators as

$$\hat{A}^{abc\cdots}_{ijk\cdots} = \hat{a}^\dagger_a \hat{a}^\dagger_b \hat{a}^\dagger_c \cdots\cdots \hat{a}_k \hat{a}_j \hat{a}_i. \tag{2}$$

Here, $a, b, c, \ldots$ are the indices for the unoccupied (virtual) spin orbitals, and $i, j, k, \ldots$ are the indices for the occupied (real) spin orbitals, and we use the standard second-quantization notation for the fermionic creation and destruction operators; note that in each $\hat{T}$ operator, all creation operators and all destruction operators are selected from the virtual orbitals and the real orbitals, respectively, and the opposite is true for the $\hat{T}^\dagger$ operators; a particular excitation-deexcitation operator in the summation appears only once—we do this by requiring the indices to be ordered $a < b < c \cdots$ and $i < j < k \cdots$.

It is important to note that carrying out a UCC calculation exactly using this method is challenging because quantum circuits for the exponential of the sum of unitaries are complicated [13]. The other method is to write down the *Ansatz* in a factorized form, given by

$$\hat{U}'_{\rm UCC} = \prod e^{\theta^{abc\cdots}_{ijk\cdots}[\hat{A}^{abc\cdots}_{ijk\cdots} - (\hat{A}^{abc\cdots}_{ijk\cdots})^\dagger]}. \tag{3}$$

Unlike the case in which we exponentiate a sum of unitaries, the factorized *Ansatz* is not uniquely determined because many of the elementary factors do not commute, leading to different results based on the ordering of the different factors. Despite this, the factorized form is still a promising approach for applying the UCC *Ansatz* on noisy intermediate-scale quantum (NISQ) machines. One reason is it can be implemented with relatively simple circuits. Using the Jordan-Wigner transformation [14,15], we convert the $\hat{A}$ and $\hat{A}^\dagger$ terms into sums of products of Pauli strings; we can immediately map the exponential of such operators into a gated circuit. The circuit requires many controlled-NOT (CNOT) gate cascades [16,17], which will lead to low-fidelity performance on current quantum hardware. Reducing the CNOT count of the factorized form of the UCC *Ansatz* could potentially allow for the use of NISQ hardware for quantum chemistry calculations.

Traditional quantum chemistry focuses primarily on single and double excitations in CC, but as the correlations grow, it is anticipated that higher-rank excitations will be needed to accurately represent the wave function. Within the classical computational chemistry framework, work by Chen *et al.* [12] created an algorithm using the factorized form of the UCC that produces significantly better results for strongly correlated systems and comparable results in terms of accuracy for weakly correlated systems. In Ref. [18], Evangelista *et al.* proved that the disentangled (factorized) UCC *Ansatz* is capable of generating arbitrary states. Reference [19] showed one can create the exact ground-state wave function for a four-site Hubbard ring (in its natural orbital basis) using a factorized form of the UCC that requires one quadruple excitation and eight double excitations. Although the circuit depth for such a state-preparation procedure is comparatively low, the one quadruple factor requires about half the gate counts for the circuit (being about an order of magnitude more gates than one doubles factor). In this work, we introduce a decomposition method that greatly reduces the gate count of costly high-rank UCC factors (such as the aforementioned quadruple excitation) into lower-rank factors.

It is important to mention that the method proposed in this paper is predicated on the fact that the fermion-to-qubit mapping used by the circuit from Ref. [18] is the Jordan-Wigner encoding. It is not universally applicable to other encodings. However, one should be able to generalize the approach given here to other fermion encodings, if desired.

II. BACKGROUND

A. Classical coupled-cluster approach

A set of electronic excitation operators can be defined as follows [20]:

$$\hat{T} = \sum_{i=1}^{N} \hat{T}_i. \tag{4}$$

Explicitly, the first two ranks (orders) are

$$\hat{T}_1 = \sum_{ia} \theta^a_i \hat{a}^\dagger_a \hat{a}_i = \sum_{ia} \theta^a_i \hat{A}^a_i, \tag{5}$$

$$\hat{T}_2 = \sum_{ijab} \theta^{ab}_{ij} \hat{a}^\dagger_a \hat{a}^\dagger_b \hat{a}_i \hat{a}_j = \sum_{ijab} \theta^{ab}_{ij} \hat{A}^{ab}_{ij}, \tag{6}$$

where $\hat{a}^\dagger_a$ is the fermionic creation operator on virtual orbital a and $\hat{a}_i$ is the fermionic annihilation operator on real orbital i and they obey the anticommutation relations as follows:

$$\{\hat{a}_i, \hat{a}_j\} = 0, \quad \{\hat{a}^\dagger_i, \hat{a}^\dagger_j\} = 0, \quad \{\hat{a}_i, \hat{a}^\dagger_j\} = \delta_{ij}, \tag{7}$$

where $\{A, B\} = AB + BA$ and δ_{ij} is the Kronecker delta function. Note that for $\hat{T}_2$ and higher-rank operators, different ordering of the indices $ijab$ can be used, but in this work, we will be using only one ordering of the indices for each equivalent term. A coupled-cluster with singles and doubles (CCSD) wave function is given by an exponential of the excitations acting on a reference state [Hartree-Fock (HF) solution],

$$|\psi_{\rm CCSD}\rangle = e^{\hat{T}_{\rm CCSD}} |\psi_0\rangle = e^{\hat{T}_1+\hat{T}_2} |\psi_0\rangle. \tag{8}$$

We compute the energy by first projecting the Schrodinger equation $H|\psi_{\rm CCSD}\rangle = E|\psi_{\rm CCSD}\rangle$ onto the HF reference $\langle\psi_0|$:

$$E = \langle\psi_0| e^{-\hat{T}_{\rm CCSD}} H e^{\hat{T}_{\rm CCSD}} |\psi_0\rangle. \tag{9}$$

We then project against a set of states $\{\langle\psi_\mu|\}$ that covers the entire space generated by $\hat{T}_{\rm CCSD}$ acting on the reference state [6,20]. The problem is solved by solving a set of nonlinear amplitude equations:

$$E = \langle\psi_0| e^{-\hat{T}_{\rm CCSD}} H e^{\hat{T}_{\rm CCSD}} |\psi_0\rangle, \tag{10}$$

$$0 = \langle\psi_\mu| e^{-\hat{T}_{\rm CCSD}} H e^{\hat{T}_{\rm CCSD}} |\psi_0\rangle. \tag{11}$$

The cost of solving these equations scales as $O(\eta^2(N-\eta)^4)$, where η is the number of electrons and N is the number of spin orbitals in the system. Note the number of amplitude equations is given by the number of amplitudes in the expansion of the $\hat{T}$ operator, which is a much smaller number than the total number of determinants in the CC wave function.

It is convenient that the operator $e^{-\hat{T}_{\rm CCSD}}He^{\hat{T}_{\rm CCSD}}$, also known as the similarity-transformed Hamiltonian, is additively separable. Combined with the fact that the exponential of the excitation $e^{\hat{T}_{\rm CCSD}}$ is multiplicatively separable, the CCSD *Ansatz* is size consistent. As mentioned previously, classical coupled-cluster theory solves the lack of size consistency of the truncated CI wave functions. Recall that the Hamiltonian in the second quantization is

$$H = \sum_{ij} h_{ij}\hat{a}_i^\dagger\hat{a}_j + \frac{1}{2}\sum_{ijkl} g_{ijkl}\hat{a}_i^\dagger\hat{a}_j^\dagger\hat{a}_k\hat{a}_l, \tag{12}$$

where h_{ij} are the one-electron integrals and g_{ijkl} are the two-electron integrals, given by

$$h_{ij} = \int dr_1 \phi_i^*(r_1)\left(-\frac{1}{2}\nabla_{r_1}^2 - \sum_{I=1}^{M}\frac{Z_I}{R_{1I}}\right)\phi_j(r_1), \tag{13}$$

$$g_{ijkl} = \int dr_1 dr_2 \phi_i^*(r_1)\phi_j^*(r_2)\frac{1}{r_{12}}\phi_k(r_1)\phi_l(r_2). \tag{14}$$

Here, M is the number of atoms in the system, Z_I are atomic numbers, $R_{1I} = |r_1 - R_I|$, $r_{12} = |r_1 - r_2|$, and $\phi(r)$ are optimized single-particle spin orbitals such as those generated by a HF calculation [21,22]. A general similarity-transformed Hamiltonian can be expanded using the Hadamard lemma, and it truncates after the fourth term $\frac{1}{24}[[[[H,T],T],T],T]$ due to the Hamiltonian having only one- and two-body interaction terms [6]. However, when acting on a multireference state, which is often needed for strongly correlated systems in order to be able to use a low-rank representation of the many-body wave function, the calculational procedure often becomes problematic.

B. Unitary coupled-cluster and disentangled UCC factors

The unitary variant of the CC method is defined as follows [9,10]:

$$|\psi_{\rm UCC}\rangle = e^{\hat{T}-\hat{T}^\dagger}|\psi_0\rangle. \tag{15}$$

The UCC method computes the energy using the variational principle:

$$E = \min_{\vec{\theta}} \frac{\langle\psi_0|\, e^{-(\hat{T}-\hat{T}^\dagger)}He^{\hat{T}-\hat{T}^\dagger}\,|\psi_0\rangle}{\langle\psi_{\rm UCC}\rangle\,\psi_{\rm UCC}}, \tag{16}$$

which requires us to work with the explicit wave function or to determine the similarity transformation of the Hamiltonian. This approach is always variational, is size consistent, and often can be extended to multireference situations. However, the Hadamard lemma expansion of its similarity-transformed Hamiltonian no longer truncates after just four terms [23,24]. Although the UCC *Ansätze* are challenging to carry out on a classical computer, a quantum computer can efficiently apply a UCC operator in its factorized form [7,25].

Implementing the UCC *Ansatz* on a quantum machine requires Trotterization as the excitation operators do not necessarily commute:

$$e^{\hat{T}-\hat{T}^\dagger} = e^{\sum_i \theta_i(\hat{A}_i - \hat{A}_i^\dagger)} \approx \left(\prod_i e^{\frac{\theta_i}{n}(\hat{A}_i - \hat{A}_i^\dagger)}\right)^n, \tag{17}$$

where θ_i is the amplitude associated with the excitation operators $\hat{A}_i$ and $\hat{A}_i^\dagger$. In the case where $n = 1$, we can write the UCC *Ansatz* as

$$|\psi'_{\rm UCC}\rangle = \prod_i e^{\theta_i(\hat{A}_i - \hat{A}_i^\dagger)}|\psi_0\rangle, \tag{18}$$

where a UCC factor then has the form $e^{\theta_i(\hat{A}_i - \hat{A}_i^\dagger)}$. One can think of this either as a crude approximation of the Trotter product or as a factorized form of the UCC *Ansatz*. It is important to note that this *Ansatz* is not unique—different orderings lead to different wave functions when the reordered factors do not commute with each other.

C. SU(2) identity for single UCC factors

A single UCC factor has a hidden SU(2) identity that exactly determines the exponential of the operator [12,18,19]. The identity follows by simply calculating powers of the exponent. We first note that

$$\begin{aligned}(\hat{A}+\hat{A}^\dagger)^2 &= \hat{A}\hat{A}^\dagger + \hat{A}^\dagger\hat{A}\\ &= \hat{n}_{a_1}\hat{n}_{a_2}\cdots\hat{n}_{a_n}\big(1-\hat{n}_{i_1}\big)\big(1-n_{i_2}\big)\cdots\big(1-\hat{n}_{i_n}\big)\\ &\quad + \big(1-\hat{n}_{a_1}\big)\big(1-\hat{n}_{a_2}\big)\cdots\big(1-\hat{n}_{a_n}\big)\hat{n}_{i_1}\hat{n}_{i_2}\cdots\hat{n}_{i_n}\end{aligned} \tag{19}$$

because $\{i, j, k, \dots\}$ and $\{a, b, c, \dots\}$ are disjoint sets. Here, $\hat{n}_\alpha = \hat{a}_\alpha^\dagger\hat{a}_\alpha$ is the number operator for spin orbital α. The cubed term can then be simplified to be

$$(\hat{A}+\hat{A}^\dagger)^3 = \hat{A}\hat{A}^\dagger\hat{A} + \hat{A}^\dagger\hat{A}\hat{A}^\dagger = \hat{A} + \hat{A}^\dagger. \tag{20}$$

This makes the power-series expansion of the exponential simple: terms with odd powers are proportional to $\hat{A}+\hat{A}^\dagger$, and terms with even powers are proportional to Eq. (19). We just have to be careful with the zeroth-power term, which is different. Hence, we have

$$\begin{aligned}&e^{\theta[\hat{A}^{a_1\cdots a_n}_{i_1\cdots i_n} - (\hat{A}^{a_1\cdots a_n}_{i_1\cdots i_n})^\dagger]}\\ &= \hat{I} + \sin\theta\big[\hat{A}^{a_1\cdots a_n}_{i_1\cdots i_n} - \big(\hat{A}^{a_1\cdots a_n}_{i_1\cdots i_n}\big)^\dagger\big]\\ &\quad + (\cos\theta - 1)\big[\hat{n}_{a_1}\hat{n}_{a_2}\cdots\hat{n}_{a_n}\big(1-\hat{n}_{i_1}\big)\\ &\quad \times \big(1-n_{i_2}\big)\cdots\big(1-\hat{n}_{i_n}\big)\\ &\quad + \big(1-\hat{n}_{a_1}\big)\big(1-\hat{n}_{a_2}\big)\cdots\big(1-\hat{n}_{a_n}\big)\hat{n}_{i_1}\hat{n}_{i_2}\cdots\hat{n}_{i_n}\big].\end{aligned} \tag{21}$$

This identity implies that when a single UCC factor acts on a state that is neither excited by $\hat{A}$ nor deexcited by $\hat{A}^\dagger$, the state is unchanged by the operator. But when the single UCC factor acts on a state that can be excited by $\hat{A}$ or deexcited by $\hat{A}^\dagger$, the result is a cosine multiplied by the original state plus a sine multiplied by the excited (or deexcited) state. It is important

TABLE I. Commutation table for all eight four-qubit Pauli strings from Eq. (23). Integers in each entry count the number of indices that anticommute.

$\{l,k,$ $j,i\}$	$XXYX$	$YXYY$	$XYYY$	$XXXY$	$YXXX$	$XYXX$	$YYYX$	$YYXY$
$XXYX$	0	2	2	2	2	2	2	4
$YXYY$	2	0	2	2	2	4	2	2
$XYYY$	2	2	0	2	4	2	2	2
$XXXY$	2	2	2	0	2	2	4	2
$YXXX$	2	2	4	2	0	2	2	2
$XYXX$	2	4	2	2	2	0	2	2
$YYYX$	2	2	2	4	2	2	0	2
$YYXY$	4	2	2	2	2	2	2	0

to note that the identity, Eq. (21), holds for *any* rank of the UCC factor.

D. Exactness of the factorized UCC circuits

In this section, we will show that the circuit for a UCC doubles factor is exact. The UCC doubles in the factorized form serve as the cornerstone of this study as we aim to decompose the high-rank operators into ones that contain primarily doubles terms.

The factorized form of the double excitation is written as

$$\hat{U}(\theta) = \exp\left[\frac{\theta_{ijkl}}{2}(\hat{a}_i^\dagger \hat{a}_j^\dagger \hat{a}_k \hat{a}_l - \hat{a}_l^\dagger \hat{a}_k^\dagger \hat{a}_j \hat{a}_i)\right]. \tag{22}$$

Here, we define the factorized UCC double excitation using the half angle $\theta_{ijkl}/2$ because this facilitates the correct rotation operators U_θ used in the quantum circuits in later sections. As discussed before, the product of these factors forms a subspace of the full Hilbert space. Although nonunique, if multiplied in a specific order, the product of these factors can be used to create very accurate trial wave functions [18,19]. To implement the UCC factors presented by Eq. (22) on quantum hardware while fully capturing the anticommutation relations shown in Eq. (7), we choose to apply the Jordan-Wigner (JW) transformation to write the fermionic operators in terms of Pauli strings [14,15,26]:

$$\begin{aligned}
&\exp\left[\frac{\theta_{ijkl}}{2}(\hat{a}_i^\dagger \hat{a}_j^\dagger \hat{a}_k \hat{a}_l - \hat{a}_l^\dagger \hat{a}_k^\dagger \hat{a}_j \hat{a}_i)\right] \\
&= \exp\left[\frac{i\theta_{ijkl}}{16}\bigotimes_{a=l+1}^{k-1} Z_a \bigotimes_{b=j+1}^{i-1} Z_b \times (X_l X_k Y_j X_i + Y_l X_k Y_j Y_i \right. \\
&\quad + X_l Y_k Y_j Y_i + X_l X_k X_j Y_i - Y_l X_k X_j X_i - X_l Y_k X_j X_i \\
&\quad \left. - Y_l Y_k Y_j X_i - Y_l Y_k X_j Y_i)\right].
\end{aligned} \tag{23}$$

Equation (23) is obtained by applying the JW transformation to Eq. (22) with the conventions $\hat{a}_n = \frac{1}{2}(X + iY) \otimes Z^{\otimes N-n-1}$ and $\hat{a}_n^\dagger = \frac{1}{2}(X - iY) \otimes Z^{\otimes N-n-1}$, where X, Y, and Z are the Pauli matrices and $0 \leqslant n \leqslant N-1$, with N being the number of qubits. The qubit state $|0\rangle$ has no electrons, and $|1\rangle$ has one electron; it is conventional to have the $|0\rangle$ state be the up-spin state and $|1\rangle$ to be the down-spin state, yielding the conventions we use for the raising and lowering operators.

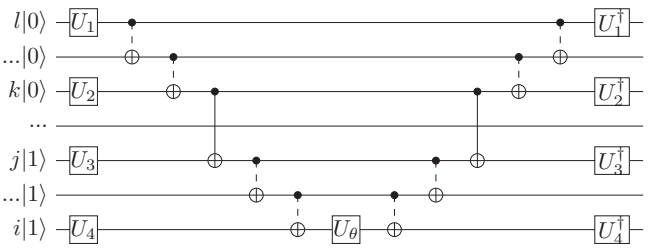

FIG. 1. Doubles UCC circuit as discussed in Refs. [16,17]. For a general doubles operator, the circuit must be applied eight times, with different combinations of U gates each time. The U-gate choices are summarized in Table III. The dashed CNOT gates are part of a CNOT cascade.

In Table I, we show that the number of anticommuting indices between the Pauli strings in Eq. (23) is always even, which implies every Pauli string commutes with every other Pauli string. This means that the exponential of the sum of the eight Pauli strings can be rewritten as eight products of the exponential of each Pauli string. The ordering of the exponential factors is unimportant because they all commute with each other. Below we provide a proof of this conclusion.

Theorem 1. Consider two Pauli strings acting on the same set of qubits,

$$P_A = \bigotimes_{i=1}^{N} A_i,\ P_B = \bigotimes_{i=1}^{N} B_i, \tag{24}$$

where $A_i, B_i \in \{X, Y, Z, I\}$. P_A and P_B commute iff A_i and B_i anticommute on an even number of indices.

Proof. Pauli matrices that do not commute anticommute. Therefore, we can write explicitly

$$P_A P_B = \bigotimes_{i=1}^{N} A_i B_i = \bigotimes_{i=1}^{N} \begin{cases} B_i A_i & \text{if } [A_i, B_i] = 0, \\ -B_i A_i & \text{if } [A_i, B_i] \neq 0. \end{cases} \tag{25}$$

The two factors A_i and B_i commute if they are both the same Pauli operator or if one of them is the identity; otherwise, they anticommute. In order for $P_A P_B$ to equal $P_B P_A$, there must be an even number of cases where $[A_i, B_i] \neq 0$ because $(-1)^{2n} = 1$. Therefore, P_A and P_B commute iff A_i and B_i anticommute on an even number of indices. ■

TABLE II. The parity is the value on qubit d after the CNOT cascade is applied.

a	b	c	d	Parity	a	b	c	d	Parity
0	0	0	0	0	0	0	0	1	1
0	0	1	0	1	0	0	1	1	0
0	1	0	0	1	0	1	0	1	0
0	1	1	0	0	0	1	1	1	1
1	0	0	0	1	1	0	0	1	0
1	0	1	0	0	1	0	1	1	1
1	1	0	0	0	1	1	0	1	1
1	1	1	0	1	1	1	1	1	0

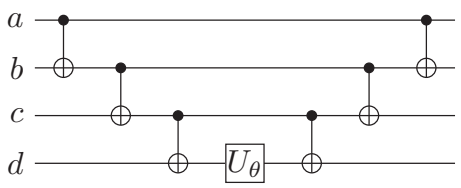

FIG. 2. Example of a circuit implementing $\exp\{-i\frac{\theta}{2}Z_a \otimes Z_b \otimes Z_c \otimes Z_d\}$ for four qubits.

Since the subterms of the UCC doubles operator all commute, the circuit shown in Fig. 1, which implements Eq. (23), is exact. In fact, a general UCC factor of order n will have 2^{2n-1} terms after the JW transformation multiplying strings of Pauli Z operators, among which numbers of Pauli X and Y operators are always odd, making numbers of anticommuting indices always even, and thus, all the strings that contain X and Y commute with one another [17].

E. The conventional quantum circuits

This section will show how one can construct the circuits for each UCC factor. The standard circuit for a single UCC doubles factor was derived in Refs. [16,17] and is shown in Fig. 1. As shown in Sec. II D, the Pauli strings in the exponentials commute. Therefore, a UCC factor can be rewritten as a product of exponentials of Pauli strings. The circuit for the UCC factors follows a prescription similar to that in [27]. Nielsen and Chuang provide a strategy for creating circuits of the form $\exp\{-i\frac{\theta}{2}Z_1Z_2\cdots Z_n\}$. By using basis transformations, one can construct a circuit for any generic Pauli string. UCC factors will use the same strategy. To construct the circuit, one can start with the circuit for evaluating $\exp\{-i\frac{\theta}{2}Z_1Z_1\cdots Z_n\}$ and then apply basis transformations to evaluate the exponential of any Pauli string.

The circuit to evaluate $\exp\{-i\frac{\theta}{2}Z_1Z_2\cdots Z_n\}$ requires a CNOT cascade, a U_θ gate applied to the last qubit, and then a reversed CNOT cascade. The CNOT cascade calculates the parity of the circuit (see Table II). After the first CNOT cascade, the last qubit in the cascade will be $|0\rangle$ if the overall parity was even and $|1\rangle$ if the parity was odd. The U_θ gate applied on the last qubit will give a phase of $\exp\{-i\theta/2\}$ if the parity is even and a phase of $\exp\{+i\theta/2\}$ if the parity is odd. The following CNOT cascade is applied to cancel out the first CNOT cascade, causing the qubits to revert to their original value, now with a resulting overall application of an exponentiated Pauli string. Figure 2 shows an example implementation of $\exp\{-i\frac{\theta}{2}Z_1Z_2Z_3Z_4\}$.

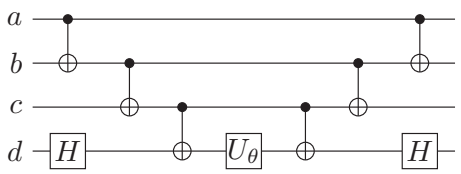

FIG. 3. Example of a circuit implementing $\exp\{-i\frac{\theta}{2}Z_a \otimes Z_b \otimes Z_c \otimes X_d\}$ for four qubits. To apply the X on a different qubit, Hadamard gates can be sandwiched around the respective qubits.

TABLE III. Eight different subcircuits that must be run sequentially to apply a UCC doubles factor to a wave function. Realizations of the generic unitary operators U_i in terms of Hadamard operators and rotations of $\pi/2$ about the x axis for each subcircuit used in the UCC doubles circuit are given in Fig. 1. The H gate converts the basis to the x basis in order to calculate the exponential of X. The $R_x(-\frac{\pi}{2})$ gate converts the basis to the y basis in order to calculate the exponential of Y. When running an exponential of Z, no basis transformation is needed. Since the relevant operators all commute, the subcircuits can be run in any order, but all eight need to appear exactly once to complete the full circuit.

Subcircuit	U_1	U_2	U_3	U_4
1	H	H	$R_x(-\frac{\pi}{2})$	H
2	$R_x(-\frac{\pi}{2})$	H	$R_x(-\frac{\pi}{2})$	$R_x(-\frac{\pi}{2})$
3	H	$R_x(-\frac{\pi}{2})$	$R_x(-\frac{\pi}{2})$	$R_x(-\frac{\pi}{2})$
4	H	H	H	$R_x(-\frac{\pi}{2})$
5	$R_x(-\frac{\pi}{2})$	H	H	H
6	H	$R_x(-\frac{\pi}{2})$	H	H
7	$R_x(-\frac{\pi}{2})$	$R_x(-\frac{\pi}{2})$	$R_x(-\frac{\pi}{2})$	H
8	$R_x(-\frac{\pi}{2})$	$R_x(-\frac{\pi}{2})$	H	$R_x(-\frac{\pi}{2})$

In order to evaluate a generic Pauli string consisting of Z, X, and Y, a basis transformation can be applied before the CNOT cascades such that the effective Pauli string is that of only Z's. If the ith gate in the Pauli string is an X, a Hadamard gate is sandwiched around the CNOT cascade on the ith qubit. This leads to the effective exponential containing a Z since $HXH = Z$. Similarly, if an exponentiated Y gate is applied, an $R_x(-\frac{\pi}{2})$ gate is sandwiched around the CNOT cascade. Figure 3 shows an example circuit to apply $\exp\{-i\frac{\theta}{2}Z_1Z_2Z_3X_4\}$. In this example, since the last Pauli in the exponentiated string is an X, a Hadamard gate is applied before and after in order to transform the basis and effectively make the circuit an exponential of Z's.

In applying the UCC *Ansatz*, circuits such as that in Fig. 1 must be rerun multiple times after applying all of the 2^{2n-1} different basis transformations [17]. A general factorized doubles UCC operator can be rewritten as Eq. (23) and implemented exactly by the circuit shown in Fig. 1 (see also Table III).

F. Control-gate identities

In order to implement some of the more complicated UCC factors needed for the decomposition method, we must break down the general control unitaries into standard gates. To get an accurate gate count of CNOTs, we use the method in Ref. [28].

Figure 4 shows the breakdown of a singly controlled unitary. A singly controlled unitary gate can be broken down into three single-qubit gates and two CNOT gates.

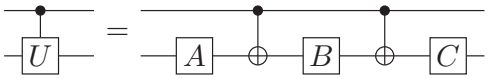

FIG. 4. Decomposition of a singly controlled unitary gate [28].

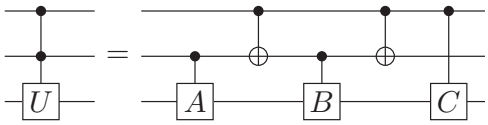

FIG. 5. Decomposition of a doubly controlled unitary gate [28].

Figure 5 shows the breakdown of a general doubly controlled unitary. A doubly controlled unitary can be broken down into three singly controlled unitaries and two CNOTs. Thus, in total, a doubly controlled unitary gate requires eight CNOT gates and nine unitaries.

III. DECOMPOSITION METHOD

We start by discussing the general schematic for the triple and quadruple excitations. We then show how one could use these schemes to generate higher-rank excitations.

The general principle for this method is as follows. In order to use mainly singles and doubles in the decomposition, we introduce ancilla orbitals. These are nonphysical orbitals that act as placeholders. We effectively create higher-rank excitations by exciting these ancilla orbitals and then applying another excitation to place them back into the correct orbitals. This is done in a way such that states that are not affected by the higher-rank excitations will remain unaffected after the full procedure is complete.

A. Quadruple excitations

We present a schematic to create a quadruple excitation using two ancilla. Our goal is to apply an operator equivalent to $\hat{A}^{wxyz}_{abcd}$. Without loss of generality, we assume that our starting state is a general state of the following form:

$$|\Psi\rangle = \xi_1 |abcd\rangle + \xi_2 |ab\phi_1\phi_2\rangle + \xi_3 |cd\phi_3\phi_4\rangle + \xi_4 |wxyz\rangle. \tag{26}$$

Here, a, b, c, d, w, x, y, and z are occupied orbitals, and ϕ_i can be any arbitrary orbital that is not a, b, c, d, w, x, y, or z. ξ_i is the coefficient associated with each state. We omit states for which the UCC factor acts like the identity and which are not touched by the operators used to construct the quadruple excitation. Note that a general state can have many terms of the form given in Eq. (26) as a linear superposition over different ϕ_i with different coefficients. But because the procedure we use is linear, those other terms will be taken care of in the circuit, so we do not need to include them explicitly in our analysis.

We illustrate the procedure graphically in Fig. 6. A UCC quadruple operator with angle θ should transform the wave function $|\Psi\rangle$ as follows:

$$\begin{aligned} &e^{\theta[\hat{A}^{wxyz}_{abcd} - (\hat{A}^{wxyz}_{abcd})^\dagger]} |\Psi\rangle \\ &\quad = \cos\theta\xi_1 |abcd\rangle + \sin\theta\xi_1 |wxyz\rangle + \xi_2 |ab\phi_1\phi_2\rangle \\ &\qquad + \xi_3 |cd\phi_3\phi_4\rangle + \cos\theta\xi_4 |wxyz\rangle - \sin\theta\xi_4 |abcd\rangle. \end{aligned} \tag{27}$$

The change in sign of the last term arises because it is a deexcitation.

The quadruple excitation requires four doubles and one double-qubit controlled UCC double operation. Table IV shows the operations used to create a quadruple excitation $\hat{A}^{wxyz}_{abcd}$. The leftmost column indicates what our target orbitals are and what they become.

Starting from our initial state, we first apply a standard doubles UCC operator that transforms $ab \to w\eta_1$ with $\theta = \pi/2$. This operator will take the occupied $|ab\rangle$ and mix it with $|w\eta_1\rangle$; it does not deexcite any state because the η_1 qubit is initially in the zero state. For example, when applied to the state $|abcd\rangle$,

$$\begin{aligned} &e^{\frac{\pi}{2}(\hat{A}^{w\eta_1}_{ab} - (\hat{A}^{w\eta_1}_{ab})^\dagger)} \xi_1 |abcd\rangle \\ &\quad = \cos\frac{\pi}{2}\xi_1 |abcd\rangle + \sin\frac{\pi}{2}\xi_1 |w\eta_1 cd\rangle = \xi_1 |w\eta_1 cd\rangle. \end{aligned} \tag{28}$$

After this operator is applied, the states $|abcd\rangle$ and $|ab\phi_1\phi_2\rangle$ will be changed. Hence, after this operation, the initial state in

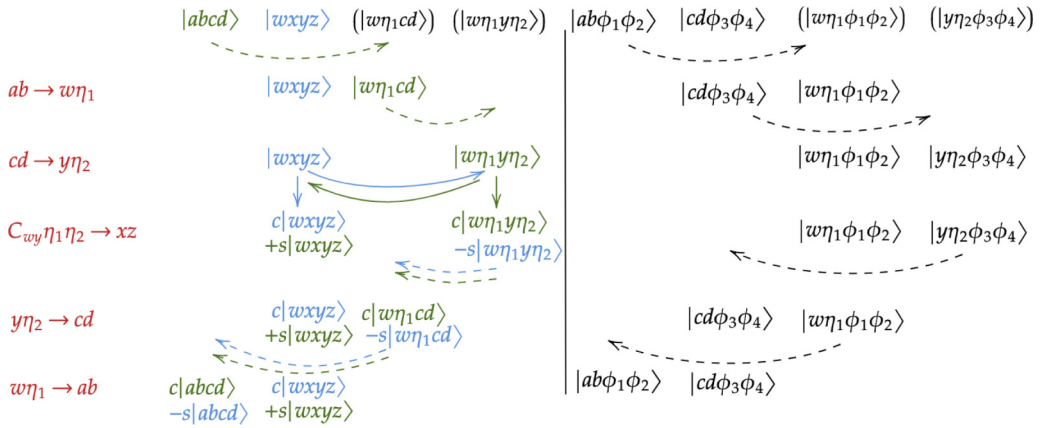

FIG. 6. Diagram for the quadruples decomposition scheme. The target states of the UCC quadruples are colored in green and blue. The four shelved states are placed on the right of the diagram. Shelved states are the ones that are not supposed to be affected by the quadruple operation, and the decomposition procedure manages to keep them intact. The states in parentheses are virtual, serving as placeholders to better illustrate some operations. Dashed lines represent full $\pi/2$ rotations, whereas solid lines represent rotations with generic angles. The coefficients c and s are cosine and sine functions of said angles from Eq. (21).

TABLE IV. Schematic for the quadruple decomposition algorithm. c and s in the second and last columns represent $\cos\theta$ and $\sin\theta$, respectively. The angles with which the four UCC doubles apply to the wave functions are all $\pi/2$, whereas the angle of the doubly controlled UCC double operator is a generic one, θ.

State	$\|abcd\rangle$	$\|ab\phi_1\phi_2\rangle$	$\|cd\phi_3\phi_4\rangle$	$\|wxyz\rangle$
$ab \to w\eta_1$	$\|w\eta_1 cd\rangle$	$\|w\eta_1\phi_1\phi_2\rangle$	$\|cd\phi_3\phi_4\rangle$	$\|wxyz\rangle$
$cd \to y\eta_2$	$\|w\eta_1 y\eta_2\rangle$	$\|w\eta_1\phi_1\phi_2\rangle$	$\|y\eta_2\phi_3\phi_4\rangle$	$\|wxyz\rangle$
$C_{wy}\eta_1\eta_2 \to xz$	$c\,\|w\eta_1 y\eta_2\rangle$	$\|w\eta_1\phi_1\phi_2\rangle$	$\|y\eta_2\phi_3\phi_4\rangle$	$c\,\|wxyz\rangle$
	$+s\,\|wxyz\rangle$			$-s\,\|w\eta_1 y\eta_2\rangle$
$y\eta_2 \to cd$	$c\,\|w\eta_1 cd\rangle$	$\|w\eta_1\phi_1\phi_2\rangle$	$\|cd\phi_3\phi_4\rangle$	$c\,\|wxyz\rangle$
	$+s\,\|wxyz\rangle$			$-s\,\|w\eta_1 cd\rangle$
$w\eta_1 \to ab$	$c\,\|abcd\rangle$	$\|ab\phi_1\phi_2\rangle$	$\|cd\phi_3\phi_4\rangle$	$c\,\|wxyz\rangle$
	$+s\,\|wxyz\rangle$			$-s\,\|abcd\rangle$

Eq. (26) is transformed into the following:

$$|\Psi\rangle \to \xi_1\,|w\eta_1 cd\rangle + \xi_2\,|w\eta_1\phi_1\phi_2\rangle + \xi_3\,|cd\phi_3\phi_4\rangle + \xi_4|wxyz\rangle. \tag{29}$$

See the top line of Fig. 6 for a summary of this first step. Next, another standard doubles UCC operator transforms $cd \to y\eta_2$ with $\theta = \pi/2$. This will change the state $|w\eta_1 cd\rangle$ to $|w\eta_1 y\eta_2\rangle$ and the state $|cd\phi_3\phi_4\rangle$ to $|y\eta_2\phi_3\phi_4\rangle$; again, there is no deexcitation because the η_2 qubit is initially in the zero state. The resulting transformed state is

$$|\Psi\rangle \to \xi_1\,|w\eta_1 y\eta_2\rangle + \xi_2\,|w\eta_1\phi_1\phi_2\rangle + \xi_3\,|y\eta_2\phi_3\phi_4\rangle + \xi_4|wxyz\rangle. \tag{30}$$

This result is summarized in the second line of Fig. 6.

The operator labeled $C_{wy}\eta_1\eta_2 \to xz$ is a doubly controlled UCC double operator. If the orbitals wy are present, then we take $\eta_1\eta_2$ and apply the UCC operator to take it to a linear superposition of xz and $\eta_1\eta_2$. The operator has a general angle θ and yields

$$\begin{aligned} &e^{\theta[\hat{A}^{xz}_{\eta_1\eta_2} - (\hat{A}^{xz}_{\eta_1\eta_2})^\dagger]}(\xi_1\,|w\eta_1 y\eta_2\rangle + \xi_4\,|wxyz\rangle) \\ &\quad = \cos\theta\xi_1\,|w\eta_1 y\eta_2\rangle + \sin\theta\xi_1\,|wxyz\rangle \\ &\qquad + \cos\theta\xi_4\,|wxyz\rangle - \sin\theta\xi_4\,|w\eta_1 y\eta_2\rangle \end{aligned} \tag{31}$$

when acting on the two states that are transformed by it. The negative sign arises because that term is a deexcitation. The

TABLE V. A seemingly working scheme that tries to decompose the UCC quadruple operator with the aid of two ancilla qubits, η_1 and η_2. Steps 1, 2, 4, and 5 are associated with angle $\theta = \pi/2$. The angle used in step 3 is arbitrary.

Step	Operation
1	$ab \to w\eta_1$
2	$cd \to y\eta_2$
3	$\eta_1\eta_2 \to xz$
4	$y\eta_2 \to cd$
5	$w\eta_1 \to ab$

TABLE VI. States of the wave function $|\Psi_{tr}\rangle$ transformed by operators from Table V. It is noticeable here that the state $|acxz\rangle$ will be affected by the critical step $\eta_1\eta_2 \to xz$ due to the fact that the UCC excitation operator is also a UCC deexcitation operator, and the resulting state will not be corrected back into $|acxz\rangle$ either. Therefore, the scheme shown in Table V fails when $|xz\phi_1\phi_2\rangle$ is present.

State	$\|abcd\rangle$	$\|acxz\rangle$	$\|abyx\rangle$	$\|cdwz\rangle$	$\|wxyz\rangle$
$ab \to w\eta_1$	$\|w\eta_1 cd\rangle$	$\|acxz\rangle$	$\|w\eta_1 yx\rangle$	$\|cdwy\rangle$	$\|wxyz\rangle$
$cd \to y\eta_2$	$\|w\eta_1 y\eta_2\rangle$	$\|acxz\rangle$	$\|w\eta_1 yx\rangle$	$\|y\eta_2 wz\rangle$	$\|wxyz\rangle$
$\eta_1\eta_2 \to xz$	$c\,\|w\eta_1 y\eta_2\rangle$	$c\,\|acxz\rangle$	$\|w\eta_1 yx\rangle$	$\|y\eta_2 wz\rangle$	$c\,\|wxyz\rangle$
	$+s\,\|wxyz\rangle$	$-s\,\|ac\eta_1\eta_2\rangle$			$-s\,\|w\eta_1 y\eta_2\rangle$
$y\eta_2 \to cd$	$c\,\|w\eta_1 cd\rangle$	$c\,\|acxz\rangle$	$\|w\eta_1 yx\rangle$	$\|cdwz\rangle$	$c\,\|wxyz\rangle$
	$+s\,\|wxyz\rangle$	$-s\,\|ac\eta_1\eta_2\rangle$			$-s\,\|w\eta_1 cd\rangle$
$w\eta_1 \to ab$	$c\,\|abcd\rangle$	$c\,\|acxz\rangle$	$\|abyx\rangle$	$\|cdwz\rangle$	$c\,\|wxyz\rangle$
	$+s\,\|wxyz\rangle$	$-s\,\|ac\eta_1\eta_2\rangle$			$-s\,\|abcd\rangle$

result after this step is

$$\begin{aligned} |\Psi\rangle \to\ &\cos\theta\xi_1\,|w\eta_1 y\eta_2\rangle + \sin\theta\xi_1\,|wxyz\rangle \\ &+ \xi_2\,|w\eta_1\phi_1\phi_2\rangle + \xi_3\,|y\eta_2\phi_3\phi_4\rangle \\ &+ \cos\theta\xi_4\,|wxyz\rangle - \sin\theta\xi_4|w\eta_1 y\eta_2\rangle. \end{aligned} \tag{32}$$

We have added in trigonometric factors, which multiply whatever the original coefficients were. This operation is depicted in the third line of Fig. 6.

The next two doubles act as corrections. They will remove the ancilla orbitals from the states. The double UCC that takes $y\eta_2 \to cd$ with $\theta = \pi/2$ changes $|y\eta_2\phi_3\phi_4\rangle$ to $|cd\phi_3\phi_4\rangle$ and $-|w\eta_1 y\eta_2\rangle \to -|w\eta_1 cd\rangle$. The state after this step is

$$\begin{aligned} |\Psi\rangle \to\ &\cos\theta\xi_1\,|w\eta_1 cd\rangle + \sin\theta\xi_1\,|wxyz\rangle \\ &+ \xi_2\,|w\eta_1\phi_1\phi_2\rangle + \xi_3\,|cd\phi_3\phi_4\rangle \\ &+ \cos\theta\xi_4\,|wxyz\rangle - \sin\theta\xi_4|w\eta_1 cd\rangle; \end{aligned} \tag{33}$$

see the second to last line of Fig. 6. Finally, the very last double takes $w\eta_1 \to ab$ with $\theta = \pi/2$. This takes the state $|w\eta_1\phi_1\phi_2\rangle$ to $|ab\phi_1\phi_2\rangle$ and $-|w\eta_1 cd\rangle$ to $-|abcd\rangle$. The final

TABLE VII. Schematic for the triple-decomposition algorithm. c and s in the second and last columns represent $\cos\theta$ and $\sin\theta$, respectively. The angles with which the four UCC doubles apply to the wave functions are all $\pi/2$, whereas the angle of the doubly controlled UCC double operator is θ.

State	$\|abc\rangle$	$\|ab\phi_1\rangle$	$\|cd\phi_2\phi_3\rangle$	$\|wxy\rangle$
$ab \to w\eta_1$	$\|w\eta_1 c\rangle$	$\|w\eta_1\phi_1\rangle$	$\|c\phi_2\phi_3\rangle$	$\|wxy\rangle$
$c \to \eta_2$	$\|w\eta_1\eta_2\rangle$	$\|w\eta_1\phi_1\rangle$	$\|\eta_2\phi_2\phi_3\rangle$	$\|wxy\rangle$
$C_w\eta_1\eta_2 \to xy$	$c\,\|w\eta_1\eta_2\rangle$	$\|w\eta_1\phi_1\rangle$	$\|\eta_2\phi_3\rangle$	$c\,\|wxy\rangle$
	$+s\,\|wxy\rangle$			$-s\,\|w\eta_1\eta_2\rangle$
$\eta_2 \to c$	$c\,\|w\eta_1 c\rangle$	$\|w\eta_1\phi_1\rangle$	$\|c\phi_2\phi_3\rangle$	$c\,\|wxy\rangle$
	$+s\,\|wxy\rangle$			$-s\,\|w\eta_1 c\rangle$
$w\eta_1 \to ab$	$c\,\|abc\rangle$	$\|ab\phi_1\rangle$	$\|c\phi_2\phi_3\rangle$	$c\,\|wxy\rangle$
	$+s\,\|wxy\rangle$			$-s\,\|abc\rangle$

TABLE VIII. Schematic for the quintuple decomposition algorithm. c and s in the second and last columns represent $\cos\theta$ and $\sin\theta$, respectively. The angles with which the four UCC doubles apply to the wave functions are all $\pi/2$, whereas the angle of the doubly controlled UCC double operator is θ.

State	$\|abcde\rangle$	$\|ab\phi_1\phi_2\phi_3\rangle$	$\|cde\phi_4\phi_5\rangle$	$\|vwxyz\rangle$
$ab \to v\eta_1$	$\|v\eta_1 cde\rangle$	$\|v\eta_1\phi_1\phi_2\phi_3\rangle$	$\|cde\phi_4\phi_5\rangle$	$\|vwxyz\rangle$
$cde \to xy\eta_2$	$\|v\eta_1 xy\eta_2\rangle$	$\|v\eta_1\phi_1\phi_2\phi_3\rangle$	$\|xy\eta_2\phi_4\phi_5\rangle$	$\|vwxyz\rangle$
$C_{vxy}\eta_1\eta_2 \to wz$	$c\,\|v\eta_1 xy\eta_2\rangle$	$\|v\eta_1\phi_1\phi_2\phi_3\rangle$	$\|xy\eta_2\phi_4\phi_5\rangle$	$c\,\|vwxyz\rangle$
	$+s\,\|vwxyz\rangle$			$-s\,\|v\eta_1 xy\eta_2\rangle$
$xy\eta_2 \to cde$	$c\,\|v\eta_1 cde\rangle$	$\|v\eta_1\phi_1\phi_2\phi_3\rangle$	$\|cde\phi_4\phi_5\rangle$	$c\,\|vwxyz\rangle$
	$+s\,\|vwxyz\rangle$			$-s\,\|v\eta_1 cde\rangle$
$v\eta_1 \to ab$	$c\,\|abcde\rangle$	$\|ab\phi_1\phi_2\phi_3\rangle$	$\|cde\phi_4\phi_5\rangle$	$c\,\|vwxyz\rangle$
	$+s\,\|vwxyz\rangle$			$-s\,\|abcde\rangle$

state is therefore

$$|\Psi\rangle \to \cos\theta\xi_1\,|abcd\rangle + \sin\theta\xi_1\,|wxyz\rangle + \xi_2\,|ab\phi_1\phi_2\rangle + \xi_3\,|cd\phi_3\phi_4\rangle + \cos\theta\xi_4\,|wxyz\rangle - \sin\theta\xi_4|abcd\rangle, \tag{34}$$

which is identical to our goal, Eq. (27); see the last line of Fig. 6 for more details.

We went through this derivation assuming there was only one term of the form $|ab\phi_1\phi_2\rangle$ in the expansion. But, of course, there can be many such terms. However, since this term gets "shelved" to a state that sits out of all the remaining UCC terms except for the last one, it should be clear that adding additional terms of this form simply shelves those additional terms (in linear superposition) and then brings them back. So this approach works for an arbitrary linear combination of terms of the form $|ab\phi_1\phi_2\rangle$. A similar conclusion can be reached for the terms of the form $|cd\phi_3\phi_4\rangle$ (with them being brought back in the second to last step).

Next, we will show that each and every step of the algorithm is necessary to successfully decompose a UCC quadruple operator.

One might assume that it is possible to break down the quad with two doubles. For example, naively applying a double that takes $ab \to wx$ and $cd \to yz$ would take $|abcd\rangle \to |wxyz\rangle$. This approach will fail even if only $|abcd\rangle$ or $|wxyz\rangle$ are present in the wave function. Suppose we have an initial wave function $|\Psi\rangle = \xi_1\,|abcd\rangle + \xi_2\,|wxyz\rangle$, where $\xi_1^2 + \xi_2^2 = 1$ and $\xi_1, \xi_2 \in \mathbb{R}$. The first step $ab \to wx$ acting on the wavefunction $|\Psi\rangle$ yields

$$|\Psi\rangle \to \cos\theta\xi_1\,|abcd\rangle + \sin\theta\xi_1\,|wxcd\rangle\cos\theta\xi_2\,|wxyz\rangle - \sin\theta\xi_2|abyz\rangle. \tag{35}$$

The second step $cd \to yz$ yields

$$\begin{aligned}|\Psi\rangle \to\ & \cos^2\theta\xi_1\,|abcd\rangle + \sin\theta\cos\theta\xi_1\,|abyz\rangle \\ & + \cos\theta\sin\theta\xi_1\,|wxcd\rangle + \sin^2\theta\xi_1\,|wxyz\rangle \\ & + \cos^2\theta\xi_2\,|wxyz\rangle - \cos\theta\sin\theta\xi_2\,|wxcd\rangle \\ & - \cos\theta\sin\theta\xi_2\,|abyz\rangle + \sin^2\theta\xi_2|abcd\rangle.\end{aligned} \tag{36}$$

Recall that the goal here is to replicate the operation

$$|\Psi\rangle \to \cos\theta\xi_1\,|abcd\rangle + \sin\theta\xi_1\,|wxyz\rangle + \cos\theta\xi_2\,|wxyz\rangle - \sin\theta\xi_2|abcd\rangle, \tag{37}$$

which the naive method fails to do.

We introduce the ancilla orbitals to circumvent such an issue. First, let us examine the scheme as shown in Table V.

Although sometimes successful at delivering the correct resulting wave functions, this method breaks down if states $|xz\phi_1\phi_2\rangle$ are present, where ϕ_i are arbitrary orbitals. For example, assume we have a wave function $|\Psi_{tr}\rangle = \xi_1\,|abcd\rangle + \xi_2\,|acxz\rangle + \xi_3\,|abyx\rangle + \xi_4\,|cdwz\rangle + \xi_5\,|wxyz\rangle$; the intermediate states obtained from using the scheme presented in Table V are shown in Table VI. Hence, a doubly controlled UCC double operation with the two control qubits placed onto orbitals w and y is used to make sure that only the state $|wxyz\rangle$ will be affected by the double $\eta_1\eta_2 \to xz$.

B. Other rank excitations

Like the quadruple excitation, the triple excitation involves five operations. We follow an architecture for the triples similar to that for the quadruple excitations. It involves two doubles, two singles, and one singly controlled double.

Table VII summarizes the operations needed to apply the triple $\hat{A}^{wxy}_{abc}$. Note that a traditional way of implementing a UCC triple operator uses fewer two-qubit gates than this method for $N \leqslant 18$; however, the gate count for CNOT gates present in the traditional circuit will quickly outnumber that in our circuit. Another direction to approach the triples is to use Givens rotations together with control gates and SWAP gates [29]. However, for large systems consisting of a large number

TABLE IX. Schematic for the 2-4 sextuple decomposition algorithm. c and s in the second and last columns represent $\cos\theta$ and $\sin\theta$, respectively. The angles with which the four UCC doubles apply to the wave functions are all $\pi/2$, whereas the angle of the doubly controlled UCC double operator is θ.

State	$\|abcdef\rangle$	$\|ab\phi_1\phi_2\phi_3\phi_4\rangle$	$\|cdef\phi_5\phi_6\rangle$	$\|uvwxyz\rangle$
$ab \to u\eta_1$	$\|u\eta_1 cdef\rangle$	$\|u\eta_1\phi_1\phi_2\phi_3\phi_4\rangle$	$\|cdef\phi_5\phi_6\rangle$	$\|uvwxyz\rangle$
$cdef \to wxy\eta_2$	$\|u\eta_1 wxy\eta_2\rangle$	$\|u\eta_1\phi_1\phi_2\phi_3\phi_4\rangle$	$\|wxy\eta_2\phi_5\phi_6\rangle$	$\|uvwxyz\rangle$
$C_{uwxy}\eta_1\eta_2 \to vz$	$c\,\|u\eta_1 wxy\eta_2\rangle$	$\|u\eta_1\phi_1\phi_2\phi_3\phi_4\rangle$	$\|wxy\eta_2\phi_5\phi_6\rangle$	$c\,\|uvwxyz\rangle$
	$+s\,\|uvwxyz\rangle$			$-s\,\|u\eta_1 wxy\eta_2\rangle$
$wxy\eta_2 \to cdef$	$c\,\|u\eta_1 cdef\rangle$	$\|u\eta_1\phi_1\phi_2\phi_3\phi_4\rangle$	$\|cdef\phi_5\phi_6\rangle$	$c\,\|uvwxyz\rangle$
	$+s\,\|uvwxyz\rangle$			$-s\,\|u\eta_1 cdef\rangle$
$u\eta_1 \to ab$	$c\,\|abcdef\rangle$	$\|ab\phi_1\phi_2\phi_3\phi_4\rangle$	$\|cdef\phi_5\phi_6\rangle$	$c\,\|uvwxyz\rangle$
	$+s\,\|uvwxyz\rangle$			$-s\,\|abcdef\rangle$

TABLE X. Schematic for the 3-3 sextuple decomposition algorithm. c and s in the second and last columns represent $\cos\theta$ and $\sin\theta$, respectively. The angles with which the four UCC doubles apply to the wave functions are all $\pi/2$, whereas the angle of the doubly controlled UCC double operator is θ.

State	$\|abcdef\rangle$	$\|abc\phi_1\phi_2\phi_3\rangle$	$\|def\phi_4\phi_5\phi_6\rangle$	$\|uvwxyz\rangle$
$abc \to uv\eta_1$	$\|uv\eta_1 def\rangle$	$\|uv\eta_1\phi_1\phi_2\phi_3\rangle$	$\|def\phi_4\phi_5\phi_6\rangle$	$\|uvwxyz\rangle$
$def \to xy\eta_2$	$\|uv\eta_1 xy\eta_2\rangle$	$\|uv\eta_1\phi_1\phi_2\phi_3\rangle$	$\|xy\eta_2\phi_4\phi_5\phi_6\rangle$	$\|uvwxyz\rangle$
$C_{uvxy}\eta_1\eta_2 \to wz$	$c\,\|uv\eta_1 xy\eta_2\rangle$	$\|uv\eta_1\phi_1\phi_2\phi_3\rangle$	$\|xy\eta_2\phi_4\phi_5\phi_6\rangle$	$c\,\|uvwxyz\rangle$
	$+s\,\|uvwxyz\rangle$			$-s\,\|uv\eta_1 xy\eta_2\rangle$
$xy\eta_2 \to def$	$c\,\|uv\eta_1 def\rangle$	$\|uv\eta_1\phi_1\phi_2\phi_3\rangle$	$\|def\phi_4\phi_5\phi_6\rangle$	$c\,\|uvwxyz\rangle$
	$+s\,\|uvwxyz\rangle$			$-s\,\|uv\eta_1 def\rangle$
$uv\eta_1 \to abc$	$c\,\|abcdef\rangle$	$\|abc\phi_1\phi_2\phi_3\rangle$	$\|def\phi_4\phi_5\phi_6\rangle$	$c\,\|uvwxyz\rangle$
	$+s\,\|uvwxyz\rangle$			$-s\,\|abcdef\rangle$

of active orbitals, multiqubit controlled SWAP gates and multiqubit Givens operators will quickly become inefficient.

For higher-rank excitations, we present various methods for decomposing N-rank excitations in terms of lower-rank excitations. While multiple methods to break down higher-rank excitations are possible, every method will follow the same methodology. We start with two excitations into ancilla orbitals, followed by a controlled operation and then two more excitations to undo the rotation into the ancilla orbitals. In total, the process takes five operations (see Table VIII). For an n-tuple excitation operator, the outer excitations should add up to n. For example, for a sextuple excitation, one should use a double and quad, two triples, or a single and a quintuple excitation.

The method of choice should depend on the hardware in use, as different methods utilize different numbers of CNOT gates and rotations. For example, consider the case of the sextuplet excitation. Either we can perform this with two doubles, two quads, and one quadruply controlled double, or we can use four triples and one quadruply controlled double. The choice to pick is based on hardware limitations, as the gate counts for different types of gates vary for these two schemes. Tables IX and X show these two schematics.

C. Code for controlled UCC factors

The decomposition method relies on controlled UCC factors. For example, in the quadruple excitation, we require a doubly controlled UCC factor that applies $\eta_1\eta_2 \to xz$ with wy as the control qubits. Figure 7 shows the circuit for a doubly controlled UCC factor; note that the circuit decomposition requires an additional two ancilla qubits, denoted α_1 and α_2. The CNOT gates applied before the unitary gates are used to encode the information of the control qubits into two ancilla qubits. In this way, even after the cascade is applied to account for the parity, qubits $|\alpha_1\rangle$ and $|\alpha_2\rangle$ contain the information from the control qubits. These qubits are not involved in the CNOT cascade but are used as control qubits for the doubly controlled rotation gate that is applied within the UCC factor.

The doubly controlled rotation gate can be broken down into unitary gates and CNOT gates [28]. A doubly controlled unitary gate can be broken down into three singly controlled unitary gates and two CNOT gates. The singly controlled unitary gates can be broken down into two CNOT gates and two unitary gates. Thus, in total, the doubly controlled unitary gates consist of eight CNOT gates and six unitaries.

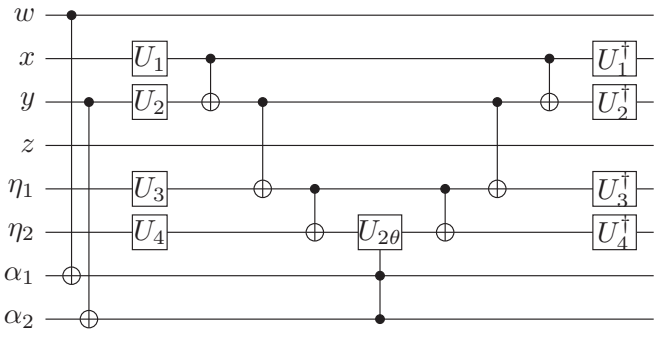

FIG. 7. Example of a circuit used to implement a doubly controlled double. This circuit corresponds to $C_{wy}\eta_1\eta_2 \to xz$. The qubits $|\alpha_1\rangle$ and $|\alpha_2\rangle$ are ancilla qubits used to keep the information of w and y since the CNOT cascade encoding parity will alter the values.

IV. RESULTS

The benefit of the decomposition method is that the total number of CNOT gates is significantly lower than what is used in a traditional N-rank UCC factor. A traditional N-rank UCC factor with M orbitals requires at most 2^{2N-1} single-qubit rotations, $2^{2N}(M-1)$ CNOT gates, and $4N(2^{2N-1})$ single-qubit nonrotation gates [16,17]. This count comes from assuming that there are no simplifications in the Jordan-Wigner strings. Each UCC factor consists of a circuit that must be run 2^{2N-1} times for an N-tuple excitation. For each run, a CNOT must be applied between every neighboring set of orbitals twice,

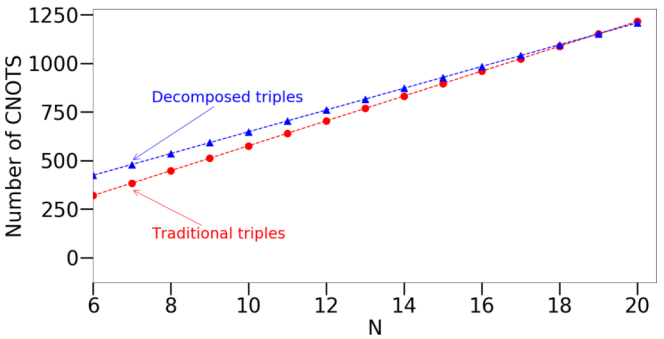

FIG. 8. CNOT gate counts of traditional triples and decomposed triples.

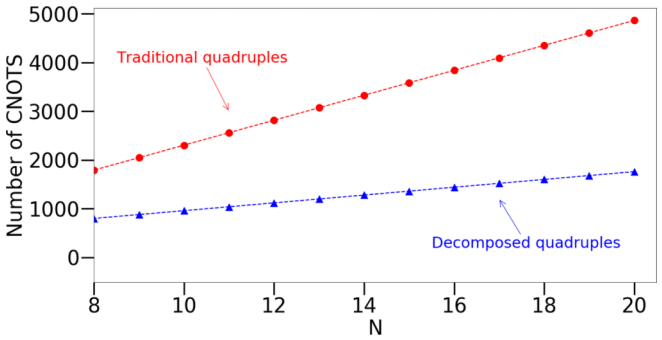

FIG. 9. CNOT gate counts of traditional quadruples and decomposed quadruples.

resulting in a total of $2(M-1)$ CNOT gates per run. In reality, the number of CNOT gates may be reduced due to simplifications in the Jordan-Wigner strings. Although this estimate for CNOT gates is generally an overestimate, the decomposition method presented above is significantly lower in gate count.

The number of CNOT counts can also be lower if one uses an encoding other than the Jordan-Wigner encoding [30]. We do not examine this strategy in detail here, primarily because such a decoding can be used for the different operators in the decomposition as well, and we anticipate similar gains in efficiency.

For comparison, consider the requirements for a quadruple excitation. A traditional quad requires 128 single-qubit rotations, $256(M-1)$ CNOT gates, and 2048 single-qubit Clifford gates. The circuit used consists of $2(M-1)$ CNOT gates from the cascade, one single-qubit rotation applied within the cascade, and 16 single-qubit gates for the basis transformations and inverse transformations. This circuit must be run 128 times.

Our decomposition instead requires two (plus two) ancilla orbitals and is built from four doubles and one doubly controlled double. The number of required qubits will increase from M to $M+4$. Two qubits are used as ancillae, and two additional qubits are needed for the controlled gate implementation. Since the decomposed quad is constructed from four doubles excitations and one controlled UCC doubles, the resulting CNOT count in the worst case is $4\times2^4[(M+2)-1]+\{2^4[(M+2)-1]+2^4\times8\}=80M+208$. The first term is the CNOT count for the four standard doubles used, and the term in the curly brackets is the count for the controlled UCC doubles. This count increases with the number of orbitals because in each of the doubles, adding an extra orbital will add two more CNOT gates to the CNOT cascade that calculates parity. The $2^4\times8$ CNOT gates come from breaking down the controlled rotation gate [28]. Note that, although we have a total of $M+4$ qubits, two of the qubits are not involved in the CNOT cascade. Compared to that of a standard quadruple, the order is much lower in the worst-case count.

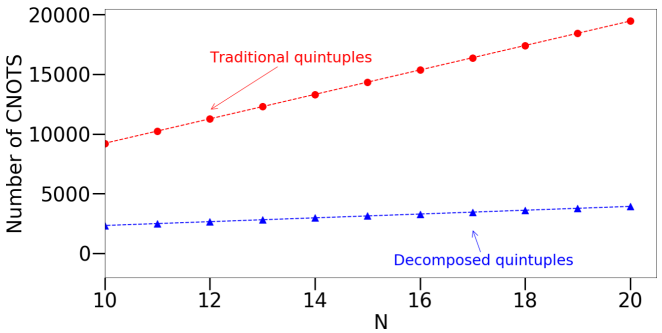

FIG. 10. CNOT gate counts of traditional quintuples and decomposed quintuples.

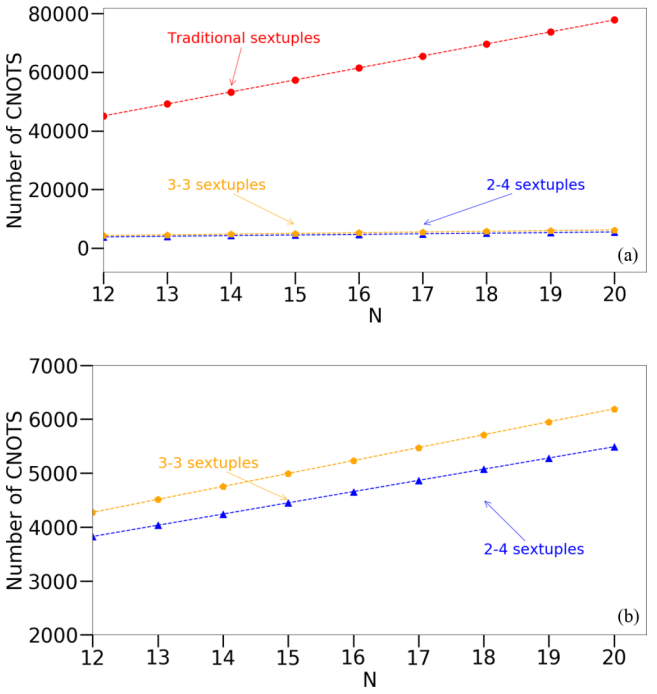

FIG. 11. (a) CNOT gate counts of traditional sextuples, the 3-3 sextuples, and the 2-4 sextuples. (b) CNOT gate counts of the 3-3 sextuples and the 2-4 sextuples.

Similarly, for other higher-rank UCC excitations, the CNOT count of the decomposition method is much lower. Figures 8–11 show the worst-case gate counts for the decomposition method against the method proposed in [16,17].

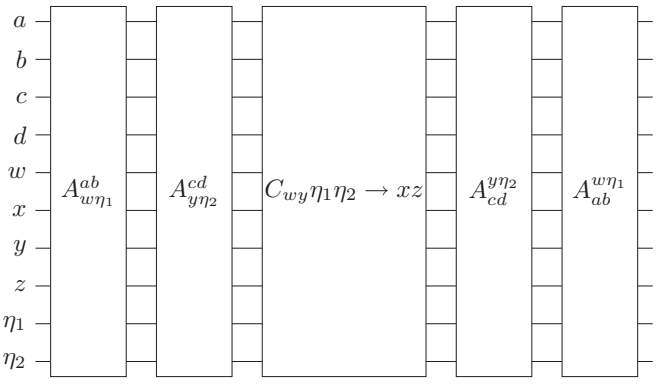

FIG. 12. Schematic of how the decomposed quad excitation would be implemented.

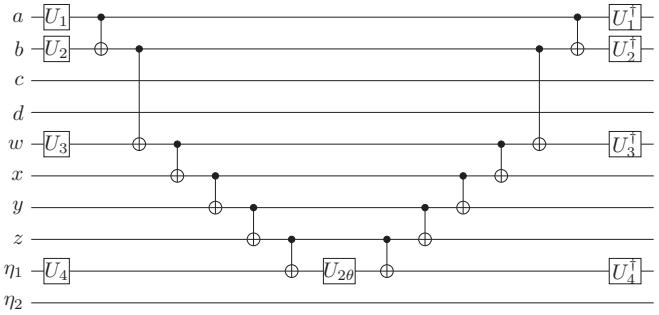

FIG. 13. Schematic of the first UCC factor in the decomposed quad.

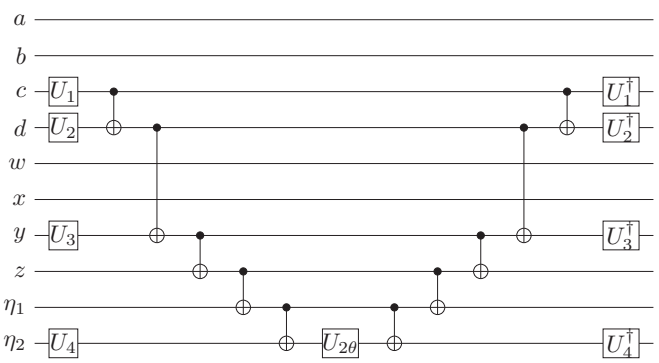

FIG. 14. Schematic of the second UCC factor in the decomposed quad.

In the NISQ era, optimizing the *Ansatz* for current hardware is necessary. In the near term, circuits that reduce circuit depth and the number of CNOT gates in exchange for a few additional qubits can be highly beneficial.

V. CONCLUSION

We have presented specific schemes to decompose high-rank UCC operators into low-rank singles and/or doubles, significantly reducing the number of CNOT gates needed to implement such circuits at the expense of using extra ancilla qubits. We have shown the proposed method is the most resource friendly when the state preparation involves entangling a large number of qubits for a large system using high-rank UCC operators, such as quintuples and sextuples (or higher). It is anticipated such terms will be needed for strongly correlated molecules that are planned to be examined on quantum computers.

For NISQ hardware, large numbers of two-qubit entangling gates are problematic. Generally, one wants to avoid having a large circuit depth due to noise, decoherence, and low fidelity. However, increasing the number of qubits in exchange for a circuit with less depth is favorable in the near term. For the construction of the specific scheme presented in this paper, we used the factorized form of the UCC *Ansatz*, which was able to create the exact ground-state wave vector using the method mentioned in [19]. Being able to decompose the UCC quadruples operator used in the state preparation for the ground-state wave function for the four-site Hubbard model at half filling, we managed to halve the total number of two-qubit gates. We anticipate that preparing strongly correlated states of larger systems, such as those studied in [31], will require higher-order UCC factors. Our approach should significantly reduce the gate counts for these circuits. Similar strategies have been used to examine the decomposition of hardware-efficient state-preparation protocols that preserve the particle number [29].

ACKNOWLEDGMENTS

We acknowledge helpful discussions with Y. Wang, R. Bennink, and E. Dumitrescu. L.X. and J.K.F. were supported by the U.S. Department of Energy, Office of Science, Office of Advanced Scientific Computing Research (ASCR), Quantum Computing Application Teams (QCATS) program, under Field Work Proposal No. ERKJ347. J.T.L. was supported by the National Science Foundation under Grant No. DMR-1659532. J.K.F. was also supported by the McDevitt bequest at Georgetown University.

APPENDIX: DECOMPOSITION OF THE STANDARD QUADRUPLE CIRCUIT

In the extended figures, we show how one may implement the decomposed quad. Figure 12 shows the generic order of UCC operators needed to implement the decomposed quad. It starts off with two doubles (indicated in Figs. 13 and 14). Then, the doubly controlled UCC doubles is applied. This circuit is given in Fig. 7. The following two blocks are the conjugate of the UCC factor of the previous two blocks. Thus, the circuit can be constructed by swapping $U_1 \leftrightarrow U_3$ and $U_2 \leftrightarrow U_4$.

[1] J. Preskill, Quantum **2**, 79 (2018).
[2] A. Aspuru-Guzik, Science **309**, 1704 (2005).
[3] S. Lloyd, Science **273**, 1073 (1996).
[4] J. Lee, W. J. Huggins, M. Head-Gordon, and K. B. Whaley, J. Chem. Theory Comput. **15**, 311 (2018).
[5] C. D. Sherrill and H. F. Schaefer, Adv. Quantum Chem. **34**, 143 (1999).
[6] R. J. Bartlett and M. Musiał, Rev. Mod. Phys. **79**, 291 (2007).
[7] A. Peruzzo, J. Mcclean, P. Shadbolt, M.-H. Yung, X.-Q. Zhou, P. J. Love, A. Aspuru-Guzik, and J. L. O'Brien, Nat. Commun. **5**, 4213 (2014).
[8] N. H. Stair and F. A. Evangelista, PRX Quantum **2**, 030301 (2021).
[9] R. J. Bartlett, S. A. Kucharski, and J. Noga, Chem. Phys. Lett. **155**, 133 (1989).
[10] H. F. Schaefer, *Methods of Electronic Structure Theory* (Springer, New York, NY, 2013).
[11] F. A. Evangelista, J. Chem. Phys. **134**, 224102 (2011).
[12] J. Chen, H.-P. Cheng, and J. K. Freericks, J. Chem. Theory Comput. **17**, 841 (2021).
[13] A. M. Childs, R. Kothari, and R. D. Somma, SIAM J. Comput. **46**, 1920 (2017).

[14] P. Jordan and E. Wigner, Z. Phys. **47**, 631 (1928).
[15] M. A. Nielsen (unpublished), https://michaelnielsen.org/blog/archive/notes/fermions_and_jordan_wigner.pdf.
[16] P. K. Barkoutsos, J. F. Gonthier, I. Sokolov, N. Moll, G. Salis, A. Fuhrer, M. Ganzhorn, D. J. Egger, M. Troyer, A. Mezzacapo, S. Filipp, and I. Tavernelli, Phys. Rev. A **98**, 022322 (2018).
[17] J. Romero, R. Babbush, J. R. Mcclean, C. Hempel, P. J. Love, and A. Aspuru-Guzik, Quantum Sci. Technol. **4**, 014008 (2018).
[18] F. A. Evangelista, G. K.-L. Chan, and G. E. Scuseria, J. Chem. Phys. **151**, 244112 (2019).
[19] L. Xu, J. T. Lee, and J. K. Freericks, Mod. Phys. Lett. B **34**, 2040049 (2020).
[20] T. J. Helgaker, *Molecular Electronic-Structure Theory* (Wiley, Hoboken, NJ, 2014).
[21] A. Szabo and N. S. Ostlund, *Modern Quantum Chemistry: Introduction to Advanced Electronic Structure Theory* (Dover, Mineola, NY, 2006).
[22] H. Taketa, S. Huzinaga, and K. O-Ohata, J. Phys. Soc. Jpn. **21**, 2313 (1966).
[23] A. G. Taube and R. J. Bartlett, Int. J. Quantum Chem. **106**, 3393 (2006).
[24] W. Kutzelnigg, Theor. Chim. Acta **80**, 349 (1991).
[25] I. O. Sokolov, P. K. Barkoutsos, P. J. Ollitrault, D. Greenberg, J. Rice, M. Pistoia, and I. Tavernelli, J. Chem. Phys. **152**, 124107 (2020).
[26] R. Somma, G. Ortiz, J. E. Gubernatis, E. Knill, and R. Laflamme, Phys. Rev. A **65**, 042323 (2002).
[27] M. A. Nielsen and I. L. Chuang, *Quantum Computation and Quantum Information* (Cambridge University Press, Cambridge, 2019).
[28] A. Barenco, C. H. Bennett, R. Cleve, D. P. DiVincenzo, N. Margolus, P. Shor, T. Sleator, J. A. Smolin, and H. Weinfurter, Phys. Rev. A **52**, 3457 (1995).
[29] J. M. Arrazola, O. Di Matteo, N. Quesada, S. Jahangiri, A. Delgado, and N. Killoran, arXiv:2106.13839.
[30] A. Anand, P. Schleich, S. Alperin-Lea, P. W. K. Jensen, S. Sim, M. Díaz-Tinoco, J. S. Kottmann, M. Degroote, A. F. Izmaylov, A. Aspuru-Guzik, arXiv:2109.15176.
[31] J. Li, Y. Yao, A. A. Holmes, M. Otten, Q. Sun, S. Sharma, and C. J. Umrigar, Phys. Rev. Res. **2**, 012015 (2020).